Advances in Aerodynamics

RESEARCH Open Access

Experimental study on transition of dynamic airfoil in pitching oscillation

Binbin Wei[1*], Yongwei Gao[2] and Shuling Hu[1]

*Correspondence:
weibinbin@xjtu.edu.cn

[1] School of Aerospace Engineering, Xi'an Jiaotong University, Xi'an 710049, China
[2] School of Aeronautics, Northwestern Polytechnical University, Xi'an 710072, China

Abstract

The transition characteristics of dynamic airfoil have significant effects on the aerodynamic performance of wind turbines, helicopter rotor blades, jet engine compressor blades, etc. The time domain and time-frequency domain characteristics of transition on a NACA0012 airfoil during its pitching oscillation were experimentally studied using wall pressure measurement technology with high time accuracy in this paper. The variable slip window technology was used to detect the transition position, and the proper orthogonal decomposition (POD) method and wavelet analysis were combined to perform the time-frequency analysis. In the gradual forward movement of the transition, the low-frequency instability is gradually enhanced by the main flow and the inverse pressure gradient, and significantly submerges the high-frequency fluctuated feature. The higher order moments of the wall pressure during dynamic airfoil transition deviate significantly from the Gaussian characteristics, which is caused by the low-frequency instability and high-frequency burst. The POD method is able to distinguish low-frequency instability from the high-frequency feature. The reduced frequency had significant effects on the transition. With the increase of the reduced frequency, the hysteresis effect of the transition became more and more significant, and the frequency component of transition was more concentrated and the energy was stronger.

Keywords: Transition, Dynamic airfoil, Fluctuating pressure, Wavelet analysis, POD

1 Introduction

Flow transition in boundary layer has always been a hot and difficult research area in the aerospace field. For a fixed wing aircraft, its aerodynamic performance is affected by the transition characteristics of the lift surface under steady condition [1]. For non-fixed wings, such as wind turbines, helicopter rotor blades, jet engine compressor blades, etc., their aerodynamic performance is affected by the unsteady transition characteristics of the profile airfoil [2, 3]. The change of transition position on dynamic airfoil will bring significant changes in aerodynamic and dynamic stall characteristics [4–10]. So, it is necessary to study the transition characteristics of dynamic airfoil.

Natural transition is the most common form of transition which generally consists of several phases with different characteristics compared to bypass transition and separation-induced transition. In the receptive phase, the disturbances in the free stream trigger the corresponding disturbances in the boundary layer in some way. The phase of

evolution of Tollmien-Schlichting (T-S) wave disturbances in the laminar flow includes both linear and nonlinear evolution of the disturbances. In the process of linear evolution, different waves evolve alone. And in the nonlinear evolution, waves interact with each other and with the free flow. In the transition phase, the amplitude of the disturbances increases sharply, the spectrum broadens sharply, and the laminar flow profile rapidly transforms into a turbulent profile.

When a laminar-turbulent transition occurs, many physical quantities will change significantly, such as boundary layer thickness, wall shear stress, wall temperature, and total pressure. Therefore, the boundary layer transition can be detected by measuring these physical quantities [11, 12]. Pascazio et al. [13] used the embedded laser velocimetry (ELV) method to study the boundary layer development of the pitching oscillation airfoil. This study has shown that the transition delay could significantly change the turbulent boundary layer behavior. Marzabadi and Soltani [14] studied the effect of surface roughness on the flow transition on a plunging oscillation airfoil. They found that the leading-edge roughness caused the transition to move forward and the turbulent boundary layer transited by the roughness did not separate from the surface due to the plunging oscillating energy of the model. Wei et al. [12] studied the transition/re-laminarization features of an S809 airfoil during its pitching oscillation using the fluctuating pressure method. They found that the transition and re-laminarization showed a significant hysteresis effect in the pitching oscillation. At small angles of attack (AoA), the hysteresis effect of aerodynamic force was mainly due to the hysteresis effect of the transition and re-laminarization.

The transition characteristics of the dynamic airfoil can have a significant impact on the dynamic stall [15]. In fact, the flow stall characteristics are different under different transition conditions, regardless of whether the flow is static or dynamic. Wilder et al. [16] studied the effect of transition on the dynamic stall and found that for an untripped model, the laminar separation bubble formation had a delay effect on the dynamic stall, and the dynamic stall is sensitive to the turbulent state in the boundary layer. Zhao et al. [17] studied the effect of transition on the dynamic stall by using CFD. The calculated results showed that the transition model affected the separation zone size and the AoA at which the separation occurred. Haghiri et al. [18] studied the dynamic stall characteristics of the SC(2)-0410 airfoil in compressible flow using wall pressure and hot film. They found that the transition hysteresis was more significant compared with that of the steady case.

In the study of the transition on dynamic airfoil, the effect of key parameters on the transition position, such as Reynolds number, Mach number [19], reduced frequency [11], average AoA and AoA amplitude [20], etc., has been studied. In the pitching oscillation, the unsteady flow transition presents significant hysteresis effect: A transition is delayed in the upstroke period, whereas it is promoted in the downstroke period. And the increase in reduced frequency [11] or AoA amplitude enhances the movement hysteresis of transition location. Unfortunately, the above-mentioned research only carried out a partial study on the transition position of the dynamic airfoil, while the studies on the statistical characteristics and the time-frequency domain characteristics of transition are still scarce.

For this reason, the transition characteristics of the NACA0012 airfoil during pitching oscillation were experimentally studied using wall pressure measurement technology with high time accuracy with a Reynolds number of $Re = 1.5 \times 10^6$ in this paper. The variable slip window technology (VSWT) was used to detect the transition position. And the statistical characteristics of the unsteady transition were studied. The proper orthogonal decomposition (POD) method and wavelet analysis were combined to perform the time-frequency analysis on the transition signal. The effects of the reduced frequency on the transition were studied.

2 Experiment and data processing

2.1 Experimental setup

The experiment was conducted in the NF-3 wind tunnel at Northwestern Polytechnical University, which is a typical large low-speed airfoil wind tunnel test section in China. The size of the airfoil test section is 8.0 m × 1.6 m × 3.0 m (length × height × width). The maximum wind speed is $U = 130$ m/s and the turbulence intensity is less than 0.05%.

The oscillation frequency of the airfoil dynamic drive mechanism could be controlled in the range of $f = 0 - 5$ Hz. The maximum angular amplitude was $A_{\max} = 15°$ and the average AoA was $\alpha = 0° - 360°$ with an accuracy of $\varepsilon \leq 6'$. The wall pressure on the airfoil surface was measured by using 32 Kulite XCQ-093 type dynamic pressure sensors, which were arranged clockwise along the middle of the model ($z/l = 0.50$), including 16 on the upper surface, 14 on the lower surface, and one on each of the leading and trailing edges. The VXI data acquisition system was used to collect the dynamic signal with a frequency response of $f_s = 20$ kHz to resolve the transition characteristics in time. The schematic diagram of the experiment is shown in Fig. 1a.

The NACA0012 airfoil with a chord length of $c = 700$ mm and a span length of $l = 1600$ mm was used to study the unsteady transition under dynamic conditions. The rotation axis was located at the position of $x/c = 0.25$. The experimental model is installed as shown in Fig. 1b.

The experimental Reynolds number based on the chord length of the airfoil was $Re = 1.5 \times 10^6$, and the free flow velocity was $U = 31.7$ m/s. To study the time-domain and time-frequency domain characteristics of transition, the motion of the airfoil was selected as a sinusoidal motion with an average AoA of $\alpha_0 = 5°$ and an amplitude of $A = 15°$. To study the effects of the reduced frequency on transition, the pitching oscillation frequencies were controlled to $f = 0.5$, 0.721, 1.0, 1.442 and 2.0 Hz, and the

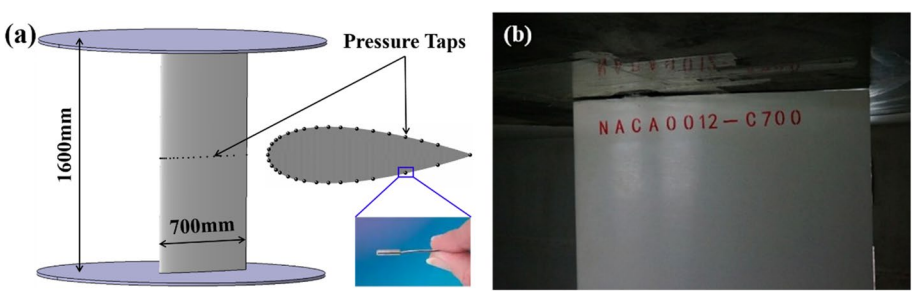

Fig. 1 Experimental scenes. **a** Schematic diagram of the experiment, **b** model installation scene

Table 1 Experimental state

Case	*c*/mm	$Re/10^6$	*k*	α_0/°	*A*/°
1	700	1.5	0.069	5	15
2	700	1.5	0.035	15	10
3	700	1.5	0.050	15	10
4	700	1.5	0.069	15	10
5	700	1.5	0.100	15	10
6	700	1.5	0.139	15	10

Table 2 Comparison of three transition detection methods

Method	Experimental time	Sampling	Accuracy of AoA	Feature detection
PA	Long, Tens of minutes	Low, Hundreds of Hz	Low	General
SWT	Short, Tens of seconds	High, Tens of kHz	Low	General
VSWT	Short, Tens of seconds	High, Tens of kHz	High	Obvious

corresponding reduced frequencies were $k=\pi fc/U=0.035$, 0.050, 0.069, 0.100, and 0.139 respectively. The detailed motion parameters are shown in Table 1.

2.2 Mathematical method

As a typical point-wise measurement method, wall pressure measurement method was used for transition detection because of its convenient operation and high frequency response [21]. Phase averaging (PA) method [11, 22–25] and slip window technology (SWT) [12] are two commonly used data processing methods for dynamic airfoil, which are suitable for different conditions. PA method is suitable for conditions with a low sampling rate and more sampling periods. In the study of Gao et al. [11], the sampling time was up to 20 minutes, and the sampling rate was only 500 Hz. While the SWT is reasonable when the sampling rate is high which can be up to 20 kHz, and the sampling period is lower [12]. However, both methods have the defects that the transition feature is not obvious and the detection accuracy of AoA at the feature position is not high. Therefore, Wei et al. [26] developed the VSWT to realize a high-precision detection of transition position. In this paper, the transition position was also detected using the VSWT. In addition, the POD method and wavelet analysis were combined to perform the time-frequency analysis on transition signal.

2.2.1 VSWT

The VSWT was essentially a kind of adaptive change window technology according to the RMS value of the fluctuating pressure. This technology further solved some shortcomings of the PA method and the SWT. The comparison of the three methods (PA, SWT, VSWT) is summarized in Table 2.

When the VSWT is performed, the calculated formula used is as follows:

$$RMS_i = \sqrt{\sum_{j=-m}^{m} \left[W\left(t_i + j\Delta t_s\right)p\left(t_i + j\Delta t_s\right) - \overline{p}_i\right]^2/(2m+1)}, \tag{1}$$

$$W = h = c_1 e^{-c_2\left(\frac{RMS}{RMS_0} - \mu_0\right)^2} + c_3, \tag{2}$$

$$m \cdot h = m_0, \tag{3}$$

where $W(t)$ is the symmetrical window function, Δt_s is the sampling period, the reciprocal of sampling frequency f_s, m is the half window width, m_0 is the reference half window width value, c_1 is the amplification factor of the window height variation function h, c_2 is the shape factor, μ_0 is the threshold value of RMS/RMS$_0$, and c_3 is the offset coefficient.

2.2.2 Wavelet analysis

To obtain the time-frequency characteristic of transition, the continuous wavelet transform (CWT) analysis of the fluctuating pressure on the airfoil surface was performed. A wavelet basis function is a set of orthogonal bases in which frequency components of a certain bandwidth are distributed near the center frequency. The complex Morlet wavelets were used as the wavelet basis functions for the CWT, which can be expressed as follows:

$$\Psi(t) = \frac{1}{\sqrt{\pi f_b}} e^{i2\pi f_c t} e^{-t^2/f_b}, \tag{4}$$

where f_b is a bandwidth parameter and f_c is a wavelet center frequency.

2.2.3 POD method

In the time-frequency analysis of fluctuating pressure signal on dynamic airfoil, the low-frequency characteristics may overwhelm the high-frequency characteristics of transition itself. Therefore, the POD method [27, 28] was considered to be used to decompose and reconstruct the fluctuating pressure signal, and then the time-frequency analysis of the reconstructed signal was performed.

Considering a pressure field $\{P\}$, look for a set of orthogonal basis $\{\varphi_j\}$, so that the element P_i in $\{P\}$ can be expressed by the following formula:

$$P_i = \sum_{j=1}^{j=M} a_j \varphi_j, \tag{5}$$

where $i = 1, 2, \ldots, M$, and M is the number of samples.

The snapshot method [29] was often used to solve this problem. After deduction, the orthogonal basis $\{\varphi_j\}$ can be expressed as:

$$\varphi = \sum_{j=1}^{M} A_j P_j. \tag{6}$$

For A_j, the eigen equation satisfies:

$$C \cdot A = \lambda \cdot A, \tag{7}$$

where $C = P^T \cdot P$.

3 Results and analysis

In this section, the time domain and time-frequency domain characteristics of transition on the NACA0012 airfoil during its pitching oscillation were studied in detail. And the effect of reduced frequency on transition was analyzed.

3.1 Time domain characteristic analysis

Taking the experimental state of $k = 0.069$, $Re = 1.5 \times 10^6$, $\alpha_0 = 5°$, $A = 15°$ (Case 1 in Table 1) as an example, the time-domain characteristics at typical positions were studied.

3.1.1 Results of VSWT

The VSWT method was used to solve the RMS value of pressure fluctuation. It is considered that the transition is featured by the RMS value peak compared with the nearby period of time. And the flow pattern in the nearby period of transition is laminar flow and turbulence, which is similar to the static criterion. Under the static condition, the

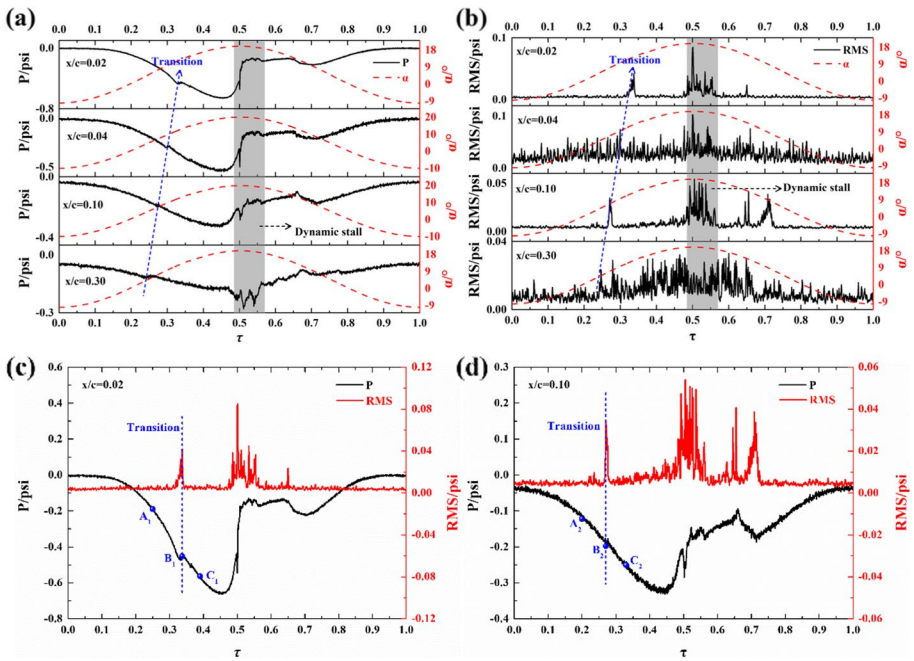

Fig. 2 Fluctuating pressure and RMS at typical positions. **a** Raw pressure signal, **b** VSWT RMS value, **c** pressure characteristics at $x/c = 0.02$, **d** pressure characteristics at $x/c = 0.10$

pressure RMS at different positions is compared, while under the dynamic condition, the RMS at different times is compared.

The raw pressure data in one period and the corresponding processing results at typical positions are shown in Fig. 2, where (a) is the raw pressure data, (b) is the RMS value calculated by VSWT, (c) is the fluctuating pressure characteristics at $x/c = 0.02$ and (d) is the fluctuating pressure characteristics at $x/c = 0.10$. The transition peak in the attached flow during upstroke could be clearly captured by using VSWT. And the transition RMS peak corresponded to the pressure inflection point during upstroke. Combined with the flow development, position A was laminar flow before position B (transition), then the turbulent flow (C) developed. With further increase in AoA, the dynamic stall occurred in the shaded area where the pressure decreased sharply, which is featured by the formation of the leading-edge vortex (LEV). During dynamic stall, a significant leading suction can be formed by such a strong coherent structure as the LEV. In addition, the strong unsteady LEV-induced pressure fluctuation can further bring large wall pressure fluctuation. Then the flow was reattached to turbulence in downstroke. The relaminarization RMS peak in downstroke can also be captured by using VSWT like the transition peak in upstroke. It is worth noting that the transition and the relaminarization were not strictly symmetrical, which was caused by the flow hysteresis.

Figure 2 clearly shows that the transition peaks of the fluctuating pressure at $x/c = 0.02$ and 0.10 are very obvious, while the transition peak at $x/c = 0.04$ is not significant, which we believe is due to the characteristics of the sensor itself. Theoretically, before the transition, there is almost no pressure fluctuation in the laminar region. And the transition process is accompanied by a nonlinear growth of the disturbance, which is characterized by a sharp increase of the pressure fluctuation. After the transition to turbulence, the pressure fluctuation gradually decreases. Therefore, if the sensor performance is extremely good, the trend of this pressure fluctuation can be captured, as shown in the results for the two positions of $x/c = 0.02$ and 0.10. However, if the sensor performance is not good enough, its own perturbation will be superimposed on the flow perturbations, which will result in the result at $x/c = 0.04$ in Fig. 2.

The pressure waveforms at different times are investigated, as shown in Fig. 3, where (a) is $x/c = 0.02$ and (b) is $x/c = 0.10$. In the figure, the colors of black, red and blue

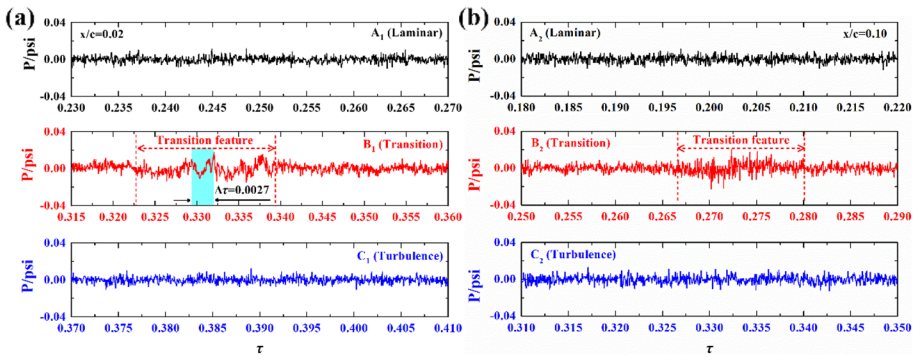

Fig. 3 Pressure waveforms at typical locations. **a** $x/c = 0.02$, **b** $x/c = 0.10$

represent the laminar flow, transition and turbulence respectively. The fluctuated feature of transition was more significant than that of laminar and turbulent flows. Its fluctuation amplitude was larger and its fluctuation intermittence was stronger. At $x/c = 0.02$, there was a significant low-frequency instability of $\Delta\tau = 0.0022$ in the transition signal as shown in Fig. 3a. And at $x/c = 0.10$, there was a significant high-frequency energy enhancement in the transition signal as shown in Fig. 3b, which indicated the occurrence of high-frequency burst. As a comparison, the pressure signals of laminar flow and turbulence were more regular in a statistical sense. The statistical characteristics of the three flow signals are investigated in the next section.

3.1.2 Statistical characteristics of the unsteady flow

To the best of the published information available to the authors, there are no studies on the statistical characteristics of the unsteady transition signal of dynamic airfoil. In this paper, the statistical characteristics of the wall pressure signal induced by the unsteady transition are investigated in terms of the probability density function (PDF) and higher order central moments.

Figure 4 shows the PDF of the normalized wall pressure at two typical locations, where the histogram is the PDF of the data in Fig. 3 and the solid blue line is the result of the standard Gaussian distribution. It can be seen that the wall pressure shows a significant Gaussian distribution for different flow conditions. In order to better characterize the degree of deviation of the data from the Gaussian distribution, the third- and fourth-order central moments of the data were calculated to characterize the skewness s and kurtosis k, respectively, as shown in Fig. 4. For both positions, the skewness of the pressure data for different flow states is almost zero, which is consistent with the Gaussian distribution. For the kurtosis, the transition signal deviates significantly from the Gaussian distribution ($k = 3.0$).

The normal probability diagram of the data in Fig. 4 is shown in Fig. 5, and the coefficient of determination R^2 was used to quantitatively evaluate the extent to which the

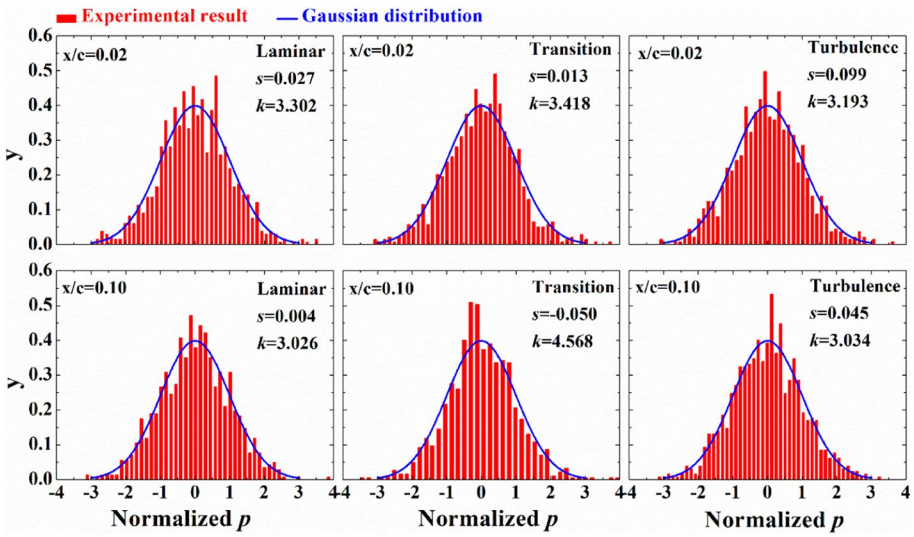

Fig. 4 Probability density function at typical locations

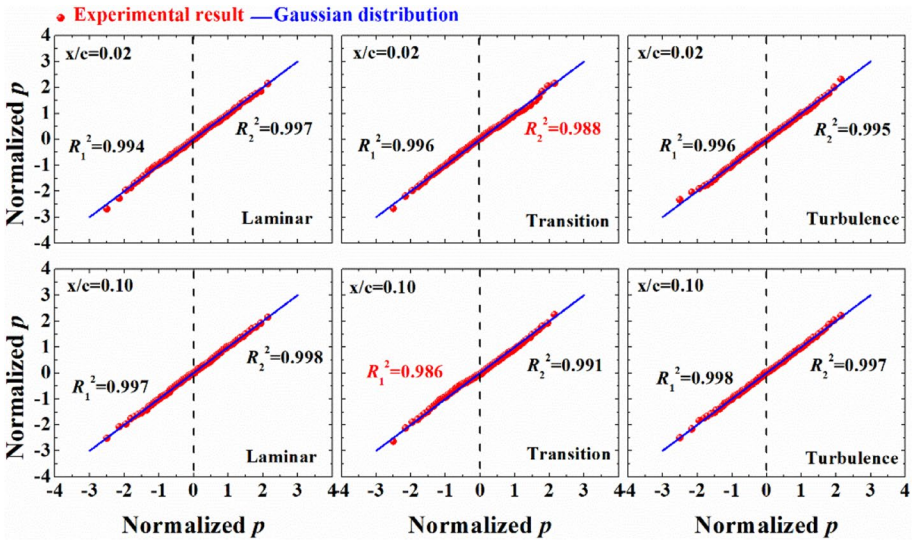

Fig. 5 Normal probability diagram at typical locations

data deviated from the Gaussian distribution. In Fig. 5, R_1^2 represents the coefficient of determination for $p<0$ and R_2^2 represents the coefficient of determination for $p>0$. For laminar and turbulent flows, both R_1^2 and R_2^2 are almost 1.0, indicating that they are extremely close to the Gaussian distribution, which is consistent with the result in Fig. 4. In contrast, for the transition, R_2^2 at the position of $x/c=0.02$ is significantly smaller than the other signals, which is caused by the low-frequency instability in the transition as shown in Fig. 3a. Similarly, R_1^2 at $x/c=0.10$ is significantly smaller than the other signals, which is caused by the high-frequency bursts in the transition at this position as shown in Fig. 3b, bringing a significant increase in the kurtosis k, as shown in Fig. 4.

As previously stated, the fluctuation or disturbance in the laminar flow is very small and difficult to be detected using the fluctuating pressure sensor, and this fluctuation will be submerged by the perturbations of the pressure sensor itself. So the Gaussian distribution of pressure fluctuation in laminar flow is from the characteristics of the pressure sensor itself. The fluctuation in the turbulence also shows a Gaussian distribution, and we believe this is caused by the large sensor range. In this paper, the unsteady pressure of the pitching oscillation airfoil was measured, and the range of the sensor at $x/c<30\%$ is large, which is 5.0 psi, in order not to damage the sensor due to the large surface suction in dynamic stall. Under such a range, the pressure fluctuation caused by the coherent structure in turbulence is difficult to be captured; therefore, the turbulence is also presented by the Gaussian characteristics in this paper.

It can be seen that during the unsteady transition of dynamic airfoil, the wall pressure shows a Gaussian like distribution, and the low-frequency instability and high-frequency burst characteristics of the transition will make the data deviate from the Gaussian distribution.

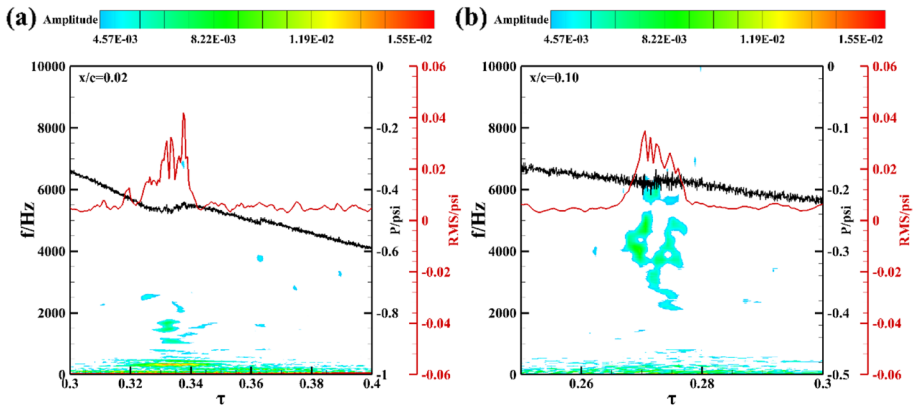

Fig. 6 Wavelet analysis at typical locations. **a** $x/c=0.02$, **b** $x/c=0.10$

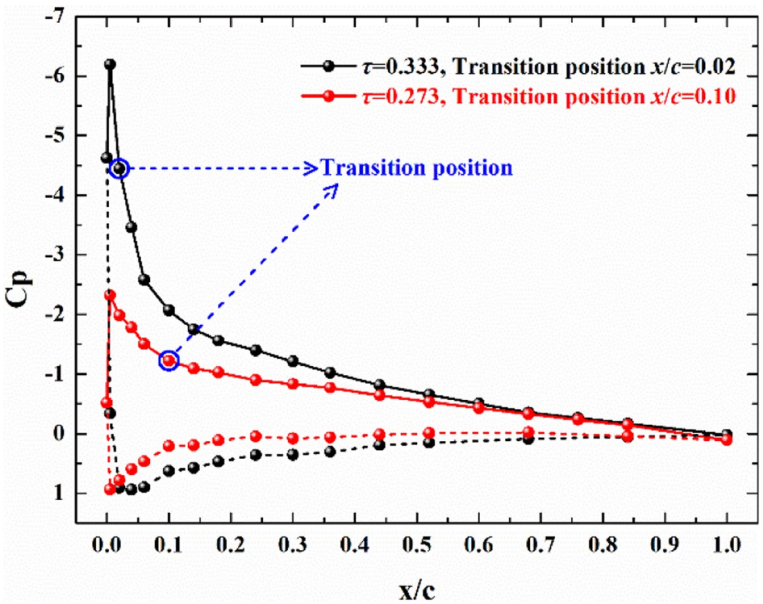

Fig. 7 C_p distributions at different AoAs

3.2 Time-frequency domain characteristic analysis

Under the dynamic condition, the wall pressure has a strong time dependence on the AoA. Both the AoA and the transition position of airfoil change as it oscillates in pitch. Specific to a measuring point, it will experience laminar flow, transition, turbulence and other flow phenomena. Therefore, time information should be considered when studying the frequency characteristics of dynamic airfoil transition. So a time-frequency analysis based on the wavelet analysis is performed in this section.

The experimental state in this section was still $k=0.069$, $Re=1.5\times10^6$, $\alpha_0=5°$, $A=15°$ (Case 1 in Table 1).

3.2.1 Wavelet analysis

The time-frequency analysis of raw pressure at typical locations was performed as shown in Fig. 6, where (a) is $x/c=0.02$ and (b) is $x/c=0.10$. In the figure, the black and

red curves are the wall pressure data and the VSWT processed RMS, respectively. When transition occurred, the energy of high-frequency signal increased significantly. The characteristic frequency of transition at $x/c=0.10$ was $f\approx 2000\,\text{Hz}-7000\,\text{Hz}$, showing significant broadband characteristics. And the characteristic frequency at $x/c=0.02$ was concentrated in $f\approx 500\,\text{Hz}-2500\,\text{Hz}$, narrowing the frequency band and reducing the frequency.

The pressure coefficient C_p distributions at two different AoAs (time) are shown in Fig. 7, where the black and red curves represent the C_p distribution when transition occurred at $x/c=0.02$ and $x/c=0.10$, respectively. The transition at $x/c=0.10$ occurred at $\tau\approx 0.273$, and the corresponding AoA was small. While the transition at $x/c=0.02$ occurred at $\tau\approx 0.333$, and the corresponding AoA was large. The transition position continued to move forward during the upstroke phase. In terms of the C_p distributions as shown in Fig. 7, the flow on the suction surface maintained attached flow at these two moments. And the transition positions were all downstream of the suction peak, reflecting a typical natural transition form of two-dimensional flows.

3.2.2 POD analysis

When the raw pressure signal was analyzed using wavelet, the high-frequency information characterizing the transition may be submerged by the low-frequency information as shown in Fig. 6a. Therefore, the POD method was used to decompose and reconstruct the pressure in this section, and then the wavelet analysis is performed on the reconstructed signal.

When using the POD method for dynamic airfoil pressure signals, the following filtering forms can be constructed [30]:

$$P_i=\sum_{j=1}^{j=M_1}a_{i,j}\varphi_j+\sum_{j=M_1+1}^{j=M}a_{i,j}\varphi_j=\overline{P_i}+\widetilde{P_i}, \tag{8}$$

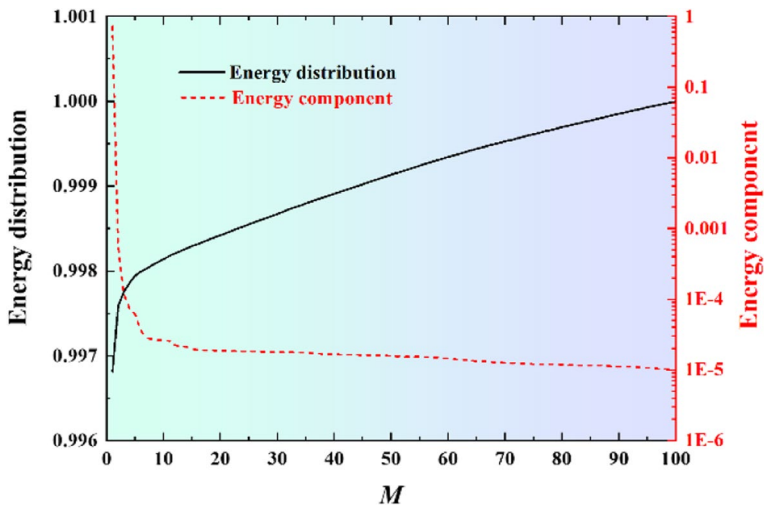

Fig. 8 Energy distribution of POD modes

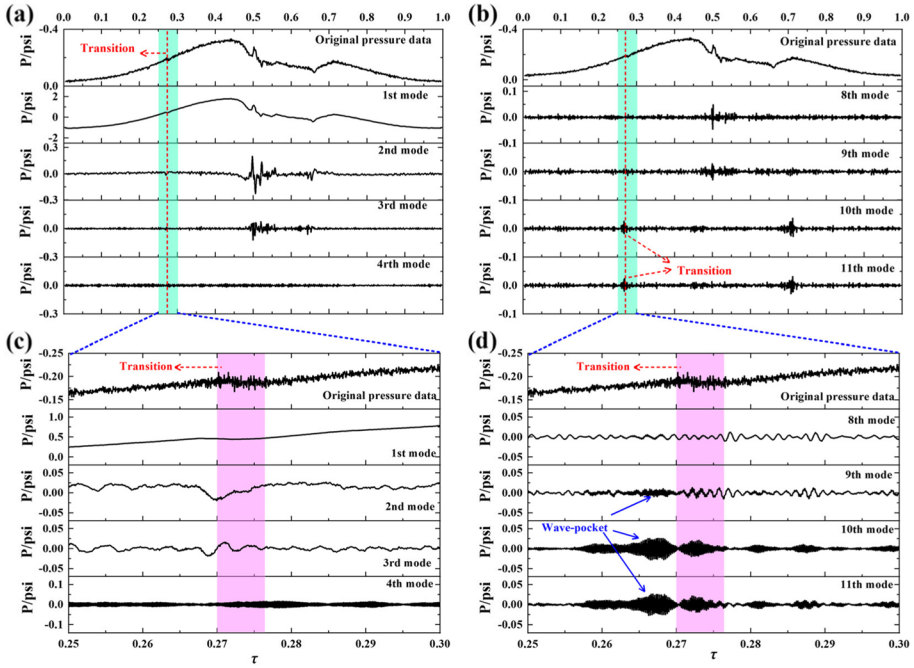

Fig. 9 POD decomposition result. **a** Global 1st – 4th modes, **b** global 8th – 11th modes, **c** local 1st – 4th modes, **d** local 8th – 11th modes

where P_i is the original signal of fluctuating pressure at the i-th measuring point, φ is a group of orthogonal bases, $\overline{P_i}$ describes the overall trend of P_i, $\widetilde{P_i}$ is the high-order fluctuation of P_i, M is the number of samples, and M_1 is the cut-off mode. In this paper, M_1 was taken as $M_1 = 5$, and the number of samples constructed was $M = 100$.

The POD modal energy distribution and the cumulative energy distribution of the wall pressure at $x/c = 0.10$ are shown in Fig. 8. The first mode occupied more than 99.6% of the total energy. And the higher modal energy accounted for a relatively low proportion, which should be related to the fluctuated characteristics of the pressure.

The comparison between the raw pressure and the typical POD modes is shown in Fig. 9. The first mode described the overall trend of the pressure induced by the model sinusoidal motion, so it contained the most energy, which could reach 99.6% (Fig. 8). The higher-order modes reflected the fluctuated characteristics of the flow, and its energy was relatively low. Specifically, the 9th to 11th orders showed the high-frequency fluctuated characteristics of transition. And there are some clear wave-packet structures and oscillations in the signals that start to appear as shown in Fig. 9d. And these wave-packet structures should be the interesting modes that potentially cause transition and break-down for that the wave-packet is accompanied by the low-frequency instability of $\Delta\tau = 0.00122$ as shown in the 9th mode. It can be seen that at the position of $x/c = 0.10$, the high-frequency fluctuated feature is significantly stronger than the low-frequency instability signal, and this low-frequency instability pattern can be resolved only after the POD decomposition. As a comparison, the low-frequency instability pattern at the position of $x/c = 0.02$ is significantly stronger than the high frequency fluctuated feature and can be resolved without POD decomposition as shown in Fig. 3a. From the perspective of time development, the transition occurs from backward to forward with the

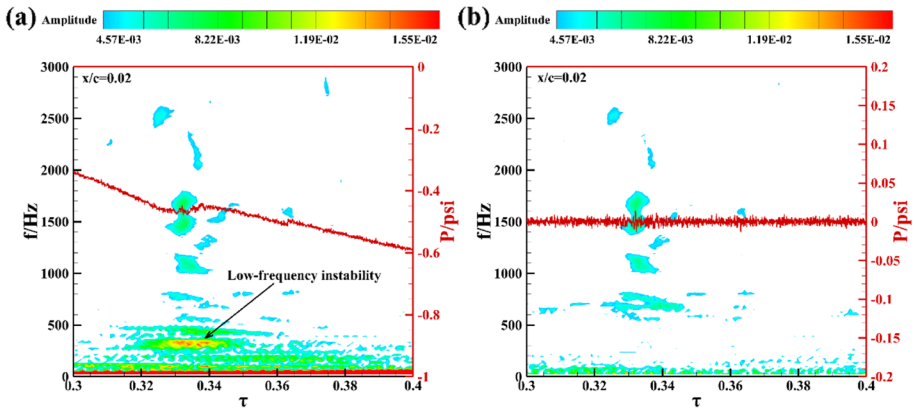

Fig. 10 Time-frequency analysis at $x/c = 0.02$. **a** Raw data, **b** high-order fluctuated data

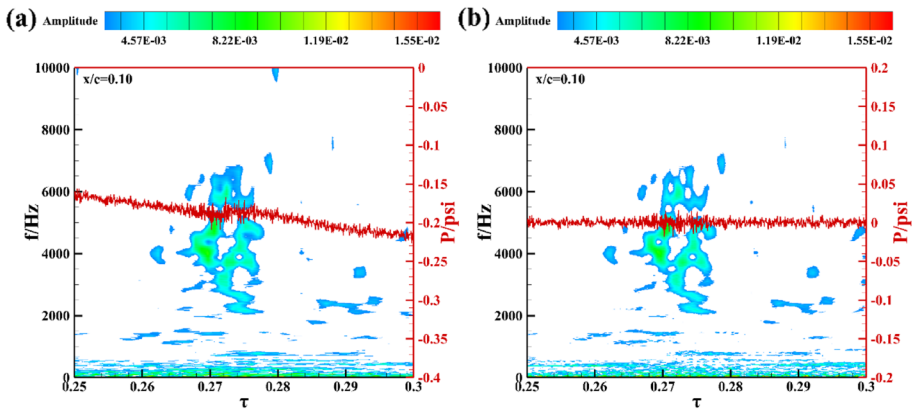

Fig. 11 Time-frequency analysis at $x/c = 0.10$. **a** Raw data, **b** high-order fluctuated data

gradual development of AoA. During the development of the transition position from $x/c = 0.10$ to $x/c = 0.02$, the low-frequency instability is gradually enhanced by the main flow and the inverse pressure gradient as shown in Fig. 7, and significantly submerges the high-frequency fluctuated feature as shown in Fig. 3a.

The time-frequency analysis of the raw pressure data and high-order POD modes reconstruction result at $x/c = 0.02$ and $x/c = 0.10$ are shown in Fig. 10 and Fig.11 respectively, where, (a) is the time-frequency analysis of the raw pressure signal and (b) is the time-frequency analysis of high-order POD modes reconstruction result. The low-frequency feature of $f \approx 370$ Hz was obvious when using the raw pressure data for wavelet analysis as shown in Fig. 10. Combined with the transitional features in Fig. 3a, it is clear that this low-frequency feature is the instability mode of transition. Combined with the POD method described in Eq. (8), the low-frequency instability features were filtered out. On the other hand, the wavelet analysis of high-order POD modes reconstruction result could better identify the high-frequency features of transition as shown in Fig. 10b and Fig. 11b.

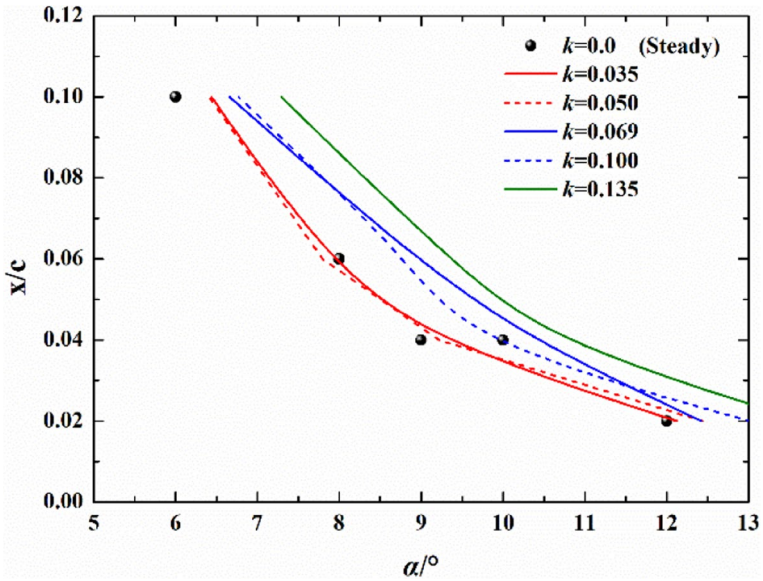

Fig. 12 Effect of reduced frequency on transition position

3.3 Effects of reduced frequency

The effects of reduced frequency on the transition of dynamic airfoil were studied in this section. The experimental states were $Re = 1.5 \times 10^6$, $\alpha_0 = 15°$, $A = 10°$ (Cases 2 – 6 in Table 1).

The effect of reduced frequency on transition position is shown in Fig. 12, where the black solid ball is the transition position under the steady condition ($k = 0$). Under the steady condition, the transition positions at AoAs of 9° and 10° were the same, which was caused by the insufficient spatial accuracy of the wall pressure detection method. The overall trend of transition positions of airfoil during pitching oscillation was consistent with that under the steady condition. With the gradual increase of AoA, the transition position moved forward gradually. Specifically, when the reduced frequency was small ($k = 0.035$ and $k = 0.050$), the dynamic transition position was basically the same as the steady transition position, reflecting the quasi-steady feature. When the reduced frequency continued to increase, the transition curve moved up obviously and showed a significant hysteresis feature. In general, the hysteresis effect of the transition increased with the increase of the reduced frequency.

The effect of reduced frequency on the time-frequency characteristics of transition was studied using the method in section 3.2.

The effect of reduced frequency on the time-frequency characteristics of transition at typical positions is shown in Fig. 13, where (a) is $x/c = 0.02$ and (b) is $x/c = 0.10$. At the position of $x/c = 0.02$, the transition feature frequency was $f \approx 500\,\text{Hz} - 2500\,\text{Hz}$, while at $x/c = 0.10$, the transition characteristic frequency was $f \approx 1500\,\text{Hz} - 7000\,\text{Hz}$. As the reduced frequency gradually increased, the transition frequency band at the two positions gradually shifted to the right (the abscissa scale was consistent), indicating that the transition was gradually delayed, which was consistent with the result in Fig. 12. During the pitching oscillation, the forward development of transition at the leading edge of

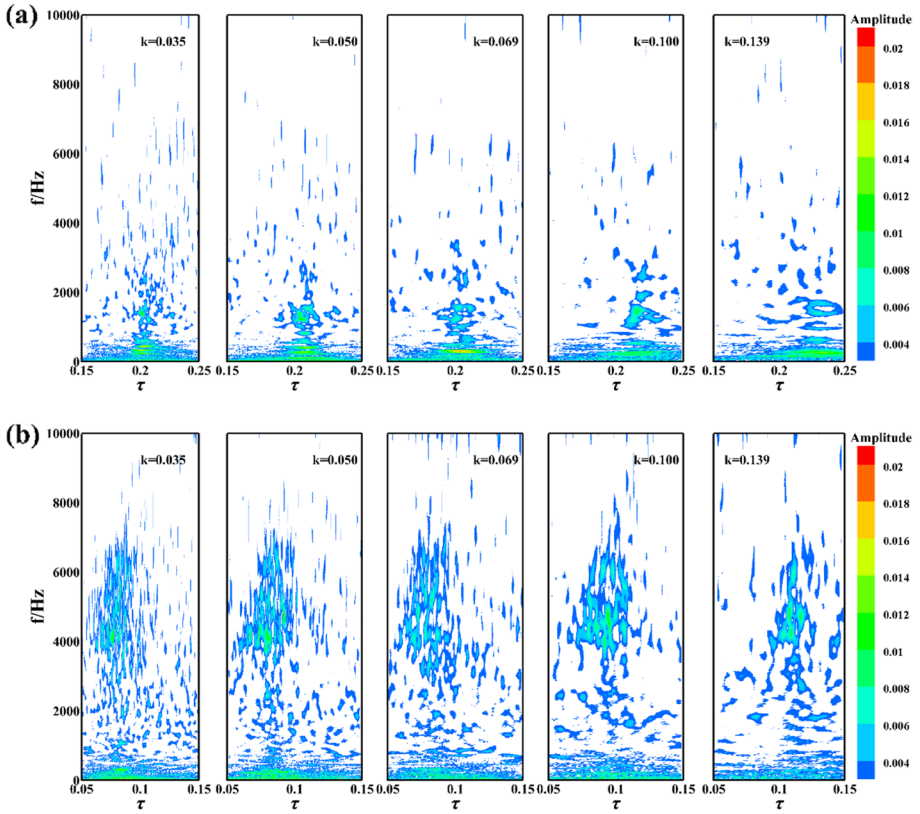

Fig. 13 Effects of reduced frequency on time-frequency characteristics of transition. **a** $x/c = 0.02$, **b** $x/c = 0.10$

airfoil ($x/c \leq 0.10$) was accompanied by frequency attenuation. In addition, at these two typical positions, the frequency component of the transition was more concentrated and the energy was stronger with the gradual increase of the reduced frequency, indicating that the increase of the reduced frequency had an effect of enhancing the characteristics of the transition frequency. In the reduced frequency range studied in this paper, the natural transitions are dominated by the T-S waves characterized by a few kilohertz.

4 Conclusion

In this paper, the time-domain and time-frequency domain characteristics of transition on a NACA0012 airfoil during its pitching oscillation were experimentally studied using wall pressure measurement technology with high time accuracy at the experimental Reynolds number of $Re = 1.5 \times 10^6$. The VSWT was used to detect the transition position. A time-frequency analysis method on transition signal combining POD and wavelet analysis was proposed. And the wavelet analysis of high-order POD modes reconstruction result could better identify the high-frequency feature.

During the pitching motion of the airfoil, the transition position gradually moved forward with the increase of the AoA. In the gradual forward movement of the transition, the low-frequency instability is gradually enhanced by the main flow and the inverse pressure gradient, and significantly submerges the high-frequency fluctuated feature.

The wall pressure during the dynamic airfoil transition shows a Gaussian like distribution, and its higher order moments deviate significantly from the Gaussian characteristics, which is caused by the low-frequency instability and high-frequency burst. The frequency of unsteady transition presented a typical broadband feature, and the transition occurring at the leading edge of the airfoil ($x/c \leq 0.10$) was accompanied by the attenuation of the characteristic frequency. The reduced frequency had a significant effect on the transition. With the reduced frequency increasing, the hysteresis effect of transition became more and more obvious. And the frequency component of transition was more concentrated and the energy was stronger.

Acknowledgements
We would like to thank all the experimental staff of the NF-3 Wind Tunnel for their hard work.

Authors' contributions
Binbin Wei: Analysis, Writing, Reviewing, Editing and Funding acquisition. Yongwei Gao and Shuling Hu: Methodology, Supervision. All authors read and approved the final manuscript.

Funding
This work was supported by the Key Laboratory of Flow Visualization and Measurement Techniques, AVIC Aerodynamics Research Institute (XFX20220502).

Availability of data and materials
The data presented in this study are available from the corresponding author upon reasonable request.

Declarations

Competing interests
The authors declare that they have no competing interests regarding this work.

Received: 4 November 2022 Accepted: 1 February 2023
Published online: 14 March 2023

References

1. Wang R, Xiao ZL (2020) Transition effects on flow characteristics around a static two-dimensional airfoil. Phys Fluids 32:035113. https://doi.org/10.1063/1.5144860
2. Liu J, Xiao ZX, Fu S (2018) Unsteady transition studies over a pitching airfoil using a *k-ω-γ* transition model. AIAA J 56(9):3776–3781. https://doi.org/10.2514/1.J056466
3. Yin TY, Pavesi G (2022) Dynamic responses of pitching hydrofoil in laminar-turbulent transition regime. J Fluids Struct 111:103544. https://doi.org/10.1016/j.jfluidstructs.2022.103544
4. Fuglsang P, Bak C, Gaunaa M et al (2004) Design and verification of the Risø-B1 airfoil family for wind turbines. J Sol Energy Eng 126(4):1002–1010. https://doi.org/10.1115/1.1766024
5. Li X, Yang K, Zhang L et al (2017) Experimental study of Reynolds number effects on performance of thick CAS wind turbine airfoils. J Renew Sustain Energ 9(6):063309. https://doi.org/10.1063/1.5018744
6. Grasso F (2016) ECN-G1-21 airfoil: design and wind-tunnel testing. J Aircr 53(5):1478–1484. https://doi.org/10.2514/1.C033089
7. Li X, Yang K, Bai J et al (2013) A method to evaluate the overall performance of the CAS-W1 airfoils for wind turbines. J Renew Sustain Energ 5(6):063118. https://doi.org/10.1063/1.4841056
8. Cooperman AM, McLennan AW, Chow R et al (2010) Aerodynamic performance of thick blunt trailing edge airfoils. Paper presented at the 28th AIAA applied aerodynamics conference, Chicago, 28 June-01 July 2010. https://doi.org/10.2514/6.2010-4228
9. BaKer JP, Mayda EA, van Dam CP (2006) Experimental and computational analysis of thick flatback wind turbine airfoils. Paper presented at the 44th AIAA aerospace sciences meeting and exhibit, Reno, 09–12 January 2006. https://doi.org/10.2514/6.2006-193
10. Freudenreich K, Kaiser K, Schaffarczyk AP et al (2004) Reynolds number and roughness effects on thick airfoils for wind turbines. Wind Eng 28(5):529–546. https://doi.org/10.1260/0309524043028109
11. Gao Y, Zhu Q, Wang L (2016) Measurement of unsteady transition on a pitching airfoil using dynamic pressure sensors. J Mech Sci Technol 30(10):4571–4578. https://doi.org/10.1007/s12206-016-0928-5
12. Wei B, Gao Y, Wang L et al (2019) Analysis of flow transition and separation on oscillating airfoil by pressure signature. J Mech Sci Technol 33:279–288. https://doi.org/10.1007/s12206-018-1227-0
13. Pascazio M, Autric J, Favier D et al (1996) Unsteady boundary-layer measurement on oscillating airfoils - transition and separation phenomena in pitching motion. Paper presented at the 34th aerospace sciences meeting and exhibit, Reno, 15-18 January 1996. https://doi.org/10.2514/6.1996-35
14. Marzabadi FR, Soltani MR (2013) Effect of leading-edge roughness on boundary layer transition of an oscillating airfoil. Sci Iran 20(3):508–515. https://doi.org/10.1016/j.scient.2012.12.035

15. Wei BB, Gao YW, Hu SL (2022) Scale effect during the dynamic stall of dynamic airfoil. Phys Fluids 34:087122. https://doi.org/10.1063/5.0098619
16. Wilder MC, Chandrasekhara MS, Carr LW (1993) Transition effects on compressible dynamic stall of transiently pitching airfoils. Paper presented at the 23rd fluid dynamics, plasmadynamics, and lasers conference, Orlando, 06–09 July 1993. https://doi.org/10.2514/6.1993-2978
17. Zhao Z, Zeng G, Wang T et al (2016) Numerical research on effect of transition on aerodynamic performance of wind turbine blade with vortex generators. J Renew Sustain Energ 8(6):063308. https://doi.org/10.1063/1.4972888
18. Haghiri AA, Mani M, Fallahpour N (2015) Unsteady boundary layer measurement on an oscillating (pitching) supercritical airfoil in compressible flow using multiple hot-film sensors. Proc Inst Mech Eng G J Aerosp Eng 229(10):1771–1784. https://doi.org/10.1177/0954410014560380
19. Richter K, Koch S, Gardner AD et al (2014) Experimental investigation of unsteady transition on a pitching rotor blade airfoil. J Am Helicopt Soc 59(1):1–12. https://doi.org/10.4050/JAHS.59.012001
20. Soltani MR, Bakhshalipour A (2008) Effect of amplitude and mean angle-of-attack on the boundary layer of an oscillating aerofoil. Aeronaut J 112(1138):705–713. https://doi.org/10.1017/S0001924000002670
21. Wei BB, Gao YW, Li D et al (2023) Supervised learning with probability interpretation in airfoil transition judgment. Chin J Aeronaut 36(1):91–104. https://doi.org/10.1016/j.cja.2022.06.013
22. Gardner AD, Richter K (2016) Transition determination on a periodic pitching airfoil using phase averaging of pressure data. In: Dillmann A, Heller G, Krämer E et al (eds) New results in numerical and experimental fluid mechanics X. Notes on numerical fluid mechanics and multidisciplinary design, vol 132. Springer, Cham. https://doi.org/10.1007/978-3-319-27279-5_26
23. Chiereghin N, Cleaver DJ, Gursul I (2019) Unsteady lift and moment of a periodically plunging airfoil. AIAA J 57(1):208–222. https://doi.org/10.2514/1.J057634
24. Gupta R, Ansell PJ (2019) Unsteady flow physics of airfoil dynamic stall. AIAA J 57(1):165–175. https://doi.org/10.2514/1.J057257
25. Li Z, Feng L, Karbasian HR et al (2019) Experimental and numerical investigation of three dimensional vortex structures of a pitching airfoil at a transitional Reynolds number. Chin J Aeronaut 32(10):2254–2266. https://doi.org/10.1016/j.cja.2019.04.015
26. Wei B, Gao Y, Li D et al (2020) Variable slip window technology in transition detection on pitching airfoil. Chin J Aeronaut 33(4):1166–1180. https://doi.org/10.1016/j.cja.2019.12.028
27. Patte-Rouland B, Lalizei G, Moreau J et al (2001) Flow analysis of an annular jet by particle image velocimetry and proper orthogonal decomposition. Meas Sci Technol 12(9):1404–1412. https://doi.org/10.1088/0957-0233/12/9/305
28. Pedersen J, Meyer K (2002) POD analysis of flow structures in a scale model of a ventilated room. Exp Fluids 33:940–949. https://doi.org/10.1007/s00348-002-0514-8
29. Sirovich L (1987) Turbulence and the dynamics of coherent structures part I: coherent structures. Q Appl Math 45(3):561–571. https://doi.org/10.1090/qam/910462
30. Wei BB, Gao YW, Li D (2021) Physics of dynamic stall vortex during pitching oscillation of dynamic airfoil. Int J Aeronaut Space Sci 22:1263–1277. https://doi.org/10.1007/s42405-021-00389-5

Publisher's Note